

PAPER

Tracing the electron motion in H_2^+ using attosecond photoelectron spectroscopy

To cite this article: Xi Chen *et al* 2021 *J. Phys. B: At. Mol. Opt. Phys.* **54** 165601

View the [article online](#) for updates and enhancements.

You may also like

- [Cardiac MRI segmentation with focal loss constrained deep residual networks](#)
Chuchen Li, Mingqiang Chen, Jinglin Zhang *et al.*
- [Commensurability condition and hierarchy of fillings for FQHE in higher Landau levels in conventional 2DEG systems and in graphene—monolayer and bilayer](#)
Janusz Jacak and Lucjan Jacak
- [Harmonic spinors on a family of Einstein manifolds](#)
Guido Franchetti



IOP | ebooks™

Bringing together innovative digital publishing with leading authors from the global scientific community.

Start exploring the collection—download the first chapter of every title for free.

Tracing the electron motion in H_2^+ using attosecond photoelectron spectroscopy

Xi Chen¹, Wei Cao^{1,*}, Zhiting Li¹, YanHong Liu¹, Kang Mi¹, Qingbin Zhang¹ and Peixiang Lu^{1,2,*}

¹ School of Physics and Wuhan National Laboratory for Optoelectronics, Huazhong University of Science and Technology, Wuhan 430074, People's Republic of China

² Hubei Key Laboratory of Optical Information and Pattern Recognition, Wuhan Institute of Technology, Wuhan 430205, People's Republic of China

E-mail: weicao@hust.edu.cn and lupeixiang@mail.hust.edu.cn

Received 20 June 2021, revised 11 August 2021

Accepted for publication 23 August 2021

Published 9 September 2021



CrossMark

Abstract

Charge migration during light–matter interaction is one of the most fundamental processes which plays a key role in chemical and biological processes of molecule. The measurement of this process requires the extreme temporal and subatomic spatial resolutions. Here, we show that a scheme based on infrared pump and short extreme ultraviolet probe technique enables us to trace the laser-controlled electron motion with high spatiotemporal resolution. By numerically solving the time-dependent Schrödinger equation for H_2^+ combined with a simple double-slit model, we demonstrate that the laser-controlled charge migration can be directly reconstructed from the interference patterns of the photoelectron spectrum.

Keywords: electron motion, attosecond photoelectron spectroscopy, interference

(Some figures may appear in colour only in the online journal)

1. Introduction

Tracing ultrafast electron motion during light–matter interaction is indispensable for understanding and manipulating the chemical and biological processes of atoms and molecules. The observation of these dynamics is the central goal of ultrafast science. As the progress in attosecond technique, it is possible to monitor and steer the electron motion on their natural timescale (10^{-18} s). Several schemes, such as attosecond transient absorption [1–3], attosecond streaking [4–6] and attosecond electron wave packet interferometry [7–9], have been successfully applied to observe these exceedingly fast processes.

Charge migration is the most fundamental photoinduced electron dynamic in chemical and biological systems and in materials. Exploring ultrafast charge migration allows one for probing electron correlation and controlling chemical reactions [10–14]. The recent work first reports the observation of charge migration in phenylalanine [15]. Charge migration

arises from a coherent superposition of the multiple electronic states, which leads to a time-dependent oscillation of the charge density in a molecule. This process can be triggered by extreme ultraviolet (XUV) excitation or by strong-field ionization generally. Charge migration immediately after ionization of iodoacetylene has been experimentally investigated using high-harmonic spectroscopy [12]. This experiment demonstrated that the position and the shape of the electron hole created by strong-field ionization can be controlled by altering the orientation of the molecule. Recently, another type of recollision-based measurement, strong-field photoelectron holography, has been applied to visualize the valence electron motion in H_2^+ with high spatial and temporal resolutions [14]. However, these recollision-based reconstruction procedures limit the time window to half an oscillating period of the laser field for visualization of electron motion.

The time-resolved pump–probe techniques have the potential to overcome this limitation. Upon projection of an initial state onto accessible excited states with an intense pump pulses in a molecule, the time evolution of the coherence can be monitored by a second delayed probe pulse, leading to

* Authors to whom any correspondence should be addressed.

the time-resolved photoelectron spectroscopy. Photoelectron spectroscopy has great potential to assess the transient molecular structure and electron dynamics. So far, the laser-induced electron diffraction has been widely used to probe the ultrafast nuclear dynamics in molecules [16–18]. Recently, the time-resolved photoelectron diffraction produced by a circularly polarized attosecond pulse has shown its potential to monitor the ultrafast charge migration in H_2^+ [23]. The migration dynamics are decoded from the asymmetric diffraction angular patterns, which indicates that the angular-resolved measurement is required for such reconstruction procedure. However, quantitative retrieval of the electron motion is yet to be implemented. In order to obtain high temporal resolution in a pump–probe experiment, the generation of ultrafast laser pulse is required generally. Despite the pulse duration is disputed, multiple groups have reported broadband soft x-ray harmonics, which correspond to the pulse duration of several tens to one hundred attosecond [19–22]. Such ultrafast laser pulse allows for the imaging of electronic motion on its natural timescale.

In the present work, we propose a new approach to image the laser-controlled charge migration in molecules by analyzing the interference patterns in photoelectron spectra generated by a linearly polarized XUV probe pulse. The prototypical molecular ion H_2^+ is used to demonstrate this method as a benchmark model. An infrared (IR) pump pulse, which creates electronic coherence between the ground state $1s\sigma_g$ and the excited state $2p\sigma_u$, is synchronized with a delayed short XUV probe pulse. This setting enables us to interrogate the laser-controlled electron dynamics. By numerically solving the time-dependent Schrödinger equation and analyzing the interference patterns of the photoelectron spectrum with a simple double-slit model, the laser-driven electron motion is completely determined with attosecond temporal and picometer spatial resolutions.

2. Principles and theoretical model

Our approach is illustrated by considering the molecular hydrogen ion H_2^+ , which can be obtained from ionization of the neutral molecule or by x-ray resonant Raman processes [24]. Theoretical model with fixed nuclear distance, which has been widely used in many researches [14, 23, 25–27], is adopted to demonstrate our proof-of-principle method. This simple model has shown its ability to provide reliable information in laser–matter interaction. We assume that the H_2^+ molecular ion is aligned. The spatial orientation control of molecules can be achieved experimentally since the molecular fragments determine the alignment with high accuracy following ionization [28, 29]. The H_2^+ is excited by an intense pump pulse to create a coherent superposition of $1s\sigma_g$ and $2p\sigma_u$ states. This leads to the asymmetric charge distribution along the molecular axis. As illustrated in the left column of figure 1(a), the evolution of molecular electron density along the internuclear axis x is displayed using one dimensional model. The pump and probe pulses are both linearly polarized along the x direction. One can observe that the electron charge is equally distributed across the two nuclei at the beginning, which indicates that

H_2^+ is in its ground state. Upon the arrival of the pump pulse, the laser–matter interaction redistributes the electron density rapidly. The electron migrates from one nucleus to the other with a period of $T = 2\pi/(E_u - E_g)$, where E_g and E_u represent the eigen-energy of $1s\sigma_g$ and $2p\sigma_u$ states, respectively. During this interaction a short XUV probe pulse is introduced and photo-ionizes the electron via single photon ionization. Superposition of the electron wave packet emitted from the two nuclei produces interference patterns whose properties depend on the molecular structure and electron distribution. This phenomenon was predicted by Cohen and Fano earlier [30]. The photoelectron spectrum detected along x axis is displayed in the right column of figure 1, which shows a modulation that assembles the seminal Young’s double slit interference. The phase as well as the depth of the modulation in the photoelectron spectrum is sensitively depending on the arrival time of the XUV pulse, corresponding to different charge distributions on the two emitters upon ionization.

Analysis of the two-center interference gives access to internuclear distance, electron distribution and phase difference between the two nuclei, which can fully determine the charge migration of H_2^+ . Suppose that the electron wavefunction in nucleus A (B) has the amplitude of $|a(t)|$ ($|b(t)|$) and the phase of ϕ_a (ϕ_b). We adopt the LCAO approximation [31], and the initial wavefunction can be written as (atomic units are used):

$$|\psi_0(r, t)\rangle = [|a(t)\rangle|\psi_{1s}(r + R/2)\rangle e^{i\phi_a(t)} + |b(t)\rangle|\psi_{1s}(r - R/2)\rangle e^{i\phi_b(t)}] e^{-iE_g t}, \quad (1)$$

with $|\psi_{1s}(r)\rangle$ being the hydrogen ground state. $e^{-iE_g t}$ represents the rapid phase evolution of the initial state. The wave packet is ionized into continuum under the plane wave approximation, where $|\psi_k(r, t)\rangle \propto e^{ikr} e^{-i\frac{k^2}{2}t}$. The transition amplitude $T(k)$ to the continuum with asymptotic momentum k can be written in velocity gauge as:

$$\begin{aligned} |T(k)|^2 &= |\text{i} \int_{-\infty}^{+\infty} \langle \psi_k(r, t) | A_X(t - t_0) \cdot \hat{p} | \psi_0(r, t) \rangle dt|^2 \\ &= |\int_{-\infty}^{+\infty} \int_{-\infty}^{+\infty} e^{-ikr} e^{i\frac{k^2}{2}t} A(t - t_0) \cdot \nabla [a(t)e^{i\phi_a(t)} \\ &\quad \times \psi(r + R/2) + b(t)e^{i\phi_b(t)}\psi(r - R/2)] e^{-iE_g t} dr dt|^2 \\ &\propto |M_{1s}(k)|^2 |E_X(k^2/2 - E_g)|^2 [|a(t_0)|^2 + |b(t_0)|^2 \\ &\quad + 2|a(t_0)||b(t_0)| \cos[kR + \phi_a(t_0) - \phi_b(t_0)]], \quad (2) \end{aligned}$$

where $A_X(t - t_0)$ is the vector potential of the XUV probe pulse and the Gaussian envelope of $A_X(t)$ has maximum at the time t_0 . \hat{p} is the momentum operator. Equation (2) describes the main characteristics of the molecular photoelectron spectrum. The intensity of the photoelectron spectrum is determined by $|M(k)|^2 |E_X(k^2/2 - E_g)|$ term, where $E_X(k^2/2 - E_g)$ represents the spectrum of XUV pulse. $M(k)$ describes the transition probability amplitude from the hydrogen ground state to the continuum with momentum k , which are accessible via quantum simulation. By normalizing the prefactor $|M(k)|^2 |E_X(k^2/2 - E_g)|$, equation (2) is reduced to a typical two-center interference

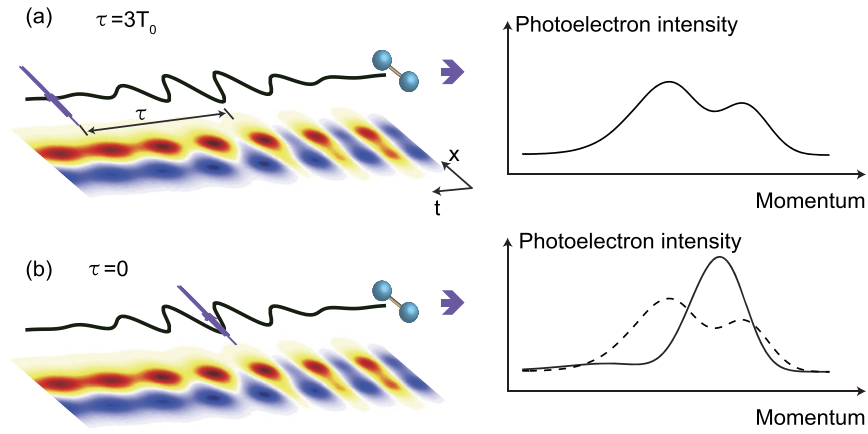


Figure 1. Schematic presentation of exploring charge migration processes in H_2^+ . The H_2^+ is aligned along x direction and the internuclear distance is fixed at $R = 5.2$ a.u.. A coherent superposition of $1s\sigma_g$ and $2p\sigma_u$ states is created and controlled by a linearly polarized pump pulse, which leads to the time evolution of electron density as shown in the left column. Subsequently a delayed XUV probe is induced to ionize the molecule. Comparing the right column of figures (a) and (b), the interference patterns are sensitively dependent on the arrival time of the XUV pulse, corresponding to different charge distributions on the two emitters upon ionization.

pattern. Note that although equation (2) can be used to well describe the photoionization process in a qualitative way, the neglecting of the Coulomb effect hinders its direct application for accurate measurement of the exceedingly fast evolution of charge distribution. The most critical point is that the momentum of the ionized electron within the Coulomb potential is not consistent with the asymptotic momentum k , and can accumulate additional phase. We define an effective momentum k_{eff} of the ionized electron, which is given by $k_{\text{eff}} = \sqrt{2(k^2/2 - E_g)}$. The meaning of the assumption is that the decrease in the electronic kinetic energy upon leaving the Coulomb potential is given by the ionization energy $-E_g$ on average [32]. By simply substituting the asymptotic momentum with the effective momentum in equation (2), the interference term can be rewritten as:

$$I(k) = |a(t_0)|^2 + |b(t_0)|^2 + 2|a(t_0)||b(t_0)| \times \cos[\sqrt{2(k^2/2 - E_g)}R + \phi_a(t_0) - \phi_b(t_0)]. \quad (3)$$

Equation (3) essentially describes the interference results of the photoelectron spectrum with satisfactory accuracy. For electrons with a particular energy, its yield corresponds to a single point in the interference pattern. Therefore, the simulated pattern is the energy spectrum of photoelectron that emitted along the laser polarization direction. It can be applied to determine the molecular charge migration using the following procedure. Firstly, destructive interference occurs when $\sqrt{2(k^2/2 - E_g)}R + \phi_a(t_0) - \phi_b(t_0) = (2n + 1)\pi$ ($n = 0, 1, \dots$). And when the H_2^+ is in its ground state, the relative phase between the two nuclei is $\Delta\phi^g = \phi_a - \phi_b = 0$. The internuclear distance R is associated with the modulation period of the photoelectron spectrum along the momentum axis, and can be directly evaluated from two adjacent interference minima in the photoelectron spectrum. Secondly, the cosine term also indicates that the variation of the relative phase between the two emitters upon photoionization shifts the interference minima. For the minimum position of

the same order, the expression is given by $\Delta\phi(t_0) - \Delta\phi^g = [k_{\text{eff}}(t_0) - k_{\text{eff}}^g]R$, where the superscript g represents that H_2^+ is in its ground state. This can help us determine the relative phase at time t_0 . Lastly, the prefactor $2|a(t_0)||b(t_0)|$ of the cosine term, which is determined by the modulation depth of the oscillation, can be easily obtained by $[I(k)_{\text{max}} - I(k)_{\text{min}}]/[I(k)_{\text{max}} + I(k)_{\text{min}}]$. $I(k)_{\text{max(min)}}$ represents the maximum (minimum) intensity of the photoelectron spectrum. Combining with the normalization condition $|a(t_0)|^2 + |b(t_0)|^2 = 1$, the electron occupation $|a(t_0)|^2$ and $|b(t_0)|^2$ can be reconstructed. The reconstructed procedure mentioned above can be applied for each delay, which can completely determine the complex-valued electron distribution on the two nuclei as a function of time, corresponding to the laser-controlled charge migration of H_2^+ .

The photoelectron spectrum is calculated by solving the time-dependent Schrödinger equation in one spatial dimension:

$$i\frac{\partial}{\partial t}\Psi(x, t) = \left[-\frac{\partial^2}{\partial x^2} + V_c(x) + V_L(t)\right]\Psi(x, t) \quad (4)$$

$V_c(x) = -1/\sqrt{(x - R/2)^2 + 1} - 1/\sqrt{(x + R/2)^2 + 1}$ is the soft-core potential of H_2^+ , which is aligned with the internuclear distance R along the x axis. The laser-molecule interaction $V_L(t) = -E(t)x$ is treated in the length gauge and dipole approximation. $E(t)$ is the electronic field consisting of a linear polarized pump pulse and a delayed XUV pulse:

$$E(t) = E_{L0}e^{-2 \ln 2(t/T_L)^2} \cos(\omega_L t) + E_{X0}e^{-2 \ln 2[(t-\tau)/T_X]^2} \cos[\omega_X(t - \tau)], \quad (5)$$

where E_{L0} (E_{X0}) and T_L (T_X) represent the amplitude and duration of the pump (probe) pulse, respectively. The polarized direction of the laser field $E(t)$ is consistent with R and τ is the time delay between the two pulses.

In the practical calculation, the initial wave function is prepared by imaginary time propagation. TDSE is integrated

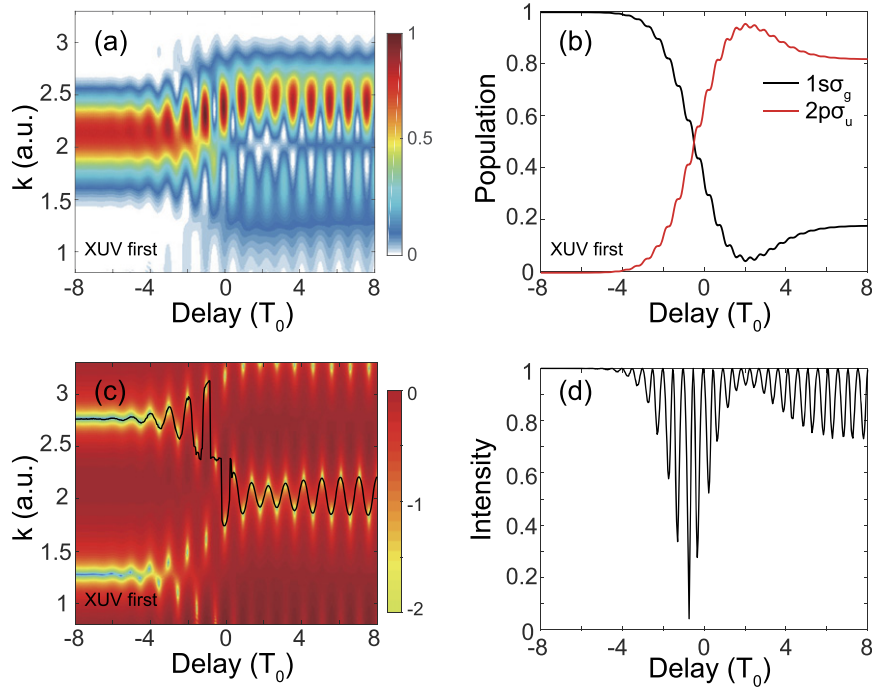


Figure 2. (a) The photoelectron spectrum of H_2^+ by using 800 nm pump pulse with the intensity of $2 \times 10^{11} \text{ W cm}^{-2}$ and a synchronized 115 eV, 40 as XUV pulse. The internuclear distance of H_2^+ is fixed at 5.2 a.u.. The label XUV first represents the XUV pulse arrives before the IR pulse. (b) Time evolution of the population $P_{1s_g}(\tau)$ and $P_{2p_u}(\tau)$ in the ground state and the excited state of the H_2^+ driven by the IR pump pulse alone. (c) The interference patterns $I(k)$ extracted from the simulated spectrum (a). Solid line presents the momentum variation of the interference minimum. The $2|a(t_0)||b(t_0)|$ term obtained by calculating $[I(k)_{\max} - I(k)_{\min}]/[I(k)_{\max} + I(k)_{\min}]$ is presented in (d).

using the split-operator spectra method [33] on a Cartesian grid from -200 to 200 a.u.. The time step is fixed at $\Delta t = 0.01$ a.u. and the spatial step is $\Delta x = 0.02$ a.u.. The photoelectron spectrum is calculated by using the wave-function splitting technique [34].

3. Results and discussions

In our simulation, a four-cycles, 800 nm IR pump with an intensity of $2 \times 10^{11} \text{ W cm}^{-2}$ is applied to start the laser-molecule interaction. Later, a linearly polarized 115 eV XUV pulse with an intensity of $1 \times 10^{12} \text{ W cm}^{-2}$ is adopted to ionized H_2^+ . The duration of the XUV field is 40 as to ensure a wider energy range of the ionized photoelectron, which is required for visualizing multiple interference minima. The simulated results show that the interference patterns of the photoelectron spectrum depend sensitively on the internuclear distance. Two types of spectra are introduced to trace the charge migration of H_2^+ . Details are presented in the following.

Figure 2(a) shows the calculated photoelectron spectrum of H_2^+ at a specific internuclear distance $R = 5.2$ atomic units (a.u.). The scenario consists of an IR pump pulse, which creates the electronic coherence between the ground and first excited states, and a delayed XUV pulse, which ionizes the electron into continuum in the present of IR pulse. As shown in figure 2(a), the photoelectron energy oscillates along the delay axis at the edge of the spectrum, which is similar to the attosecond streaking experiment. In addition to this, the results show completely different features compared with attosecond

streaking. Apparently, the photoelectron distribution gradually splits into two parts with the increase of delay [35]. A distinct minimum of the electron distribution appears at around zero delay and starts oscillating along the delay axis. Moreover, quantum beat signals appear, which are attributed to the ionization from multiple bound states. All the features in the photoelectron spectrum are induced by the resonant transition between $1s_g$ and $2p_u$ electronic states. A qualitative interpretation is given based on figure 2(b). At $R = 5.2$ a.u., the molecular eigen-energy for the ground state $1s_g$ and the first excited state $2p_u$ are $E_g = -0.898$ a.u. and $E_u = -0.841$ a.u., respectively. The pump pulse has a central energy $\omega_{\text{pu}} = 0.057$ a.u.. Figure 2(b) illustrates the time evolution of the populations $P_{1s_g}(t) = |\langle \psi_{1s_g}(x) | \psi(x, t) \rangle|^2$ and $P_{2p_u}(t) = |\langle \psi_{2p_u}(x) | \psi(x, t) \rangle|^2$. It shows a clear inversion between $1s_g$ and $2p_u$ states which is caused by a laser-driven Rabi process. It can qualitatively explain the structures of the photoelectron spectrum in figure 2(a). The ground $1s_g$ state and the excited $2p_u$ state have different symmetries: $\psi_{1s_g}(x) = \psi_{1s_g}(-x)$ for the ground state and $\psi_{2p_u}(x) = -\psi_{2p_u}(-x)$ for the excited state, which corresponds to a π phase difference of $\phi_a(t_0) - \phi_b(t_0)$ when electrons are ionized from these two different states. Thus, the momentum position of the destructive interference of $1s_g$ coincides with the constructive interference of $2p_u$. At delay $= -8T_0$ in figure 2(a), it is easy to calculate from equation (3) that constructive interference occurs around $k = 2$ a.u.. With the increase of the population of $2p_u$ state, the momentum of interference minima changes along the delay axis. Later, destructive

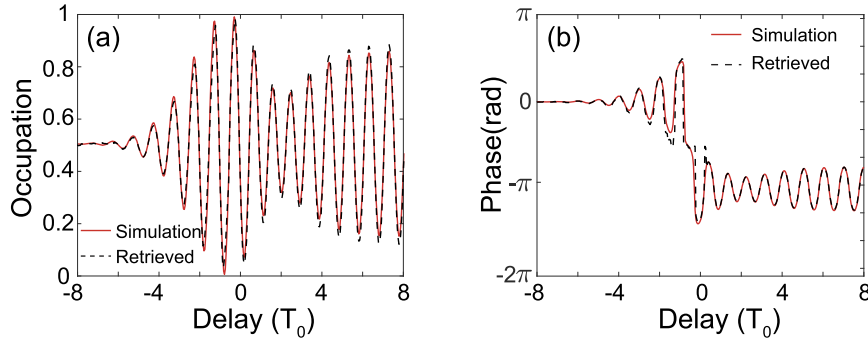


Figure 3. Reconstructed results of the charge migration in H_2^+ at $R = 5.2$ a.u. (a) Time evolution of the electron occupation in one of the nuclei. The red solid line and the dashed line represent the simulated and retrieved results, respectively. (b) The delay-dependent phase difference of the wave function on the two nuclei. The reconstructed (dashed line) and simulated (red solid line) results show a great agreement.

interference occurs at the same momentum ($k = 2$ a.u.) and delay = 0, which corresponds to the cross point of the two time-dependent populations. At positive delays, the destructive interference results in the splitting of photoelectron spectrum, which indicates that the electron population is dominated by the $2p\sigma_u$ state. Secondly, quantum beat signals appear as long as the superposition of $1s\sigma_g$ and $2p\sigma_u$ states is formed. The interference between photoelectrons ionized from two pathways leads to the oscillating structure, with the period determined by the energy difference of the two involved states.

These characters in the photoelectron spectrum are essentially determined by the separation, amplitudes and phases of the electron wave function located on the two nuclei. As discussed in section 2, equation (3) is a quantitative description of the photoelectron spectrum, which can be applied to trace laser-controlled electron motion. Note that equation (3) describes a photoelectron spectrum without considering the effect of the IR pulse on free electrons. When applying the reconstruction procedure, it is important to eliminate the ‘streaking’ effect on the spectrum. The ‘streaking’ effect describes the momentum shift of an electron ionized into a laser-dressed continuum which is given by $\Delta k = A_{\text{pu}}(\tau)$ according to the momentum conservation [36]. $A_{\text{pu}}(\tau)$ is the vector potential of the IR pulse at ionization time. The pure interference term $I(k)$ in figure 2(a) is accessible by eliminating the ‘streaking’ effect and then dividing the spectrum by the $|M_{1s}(k)|^2 |E_X(k^2/2 - E_g)|^2$ term as described in the principle. The result is displayed in figure 2(c), where the intensity of the photoelectron spectrum is in logarithmic scale for clearly observing the variation of interference minima.

The 2D spectrogram of figure 2(c) contains a wealth of structural and dynamic information of the laser-driven charge migration process, which can be accurately retrieved using equation (3). There are two interference minima at large negative delays in figure 2(c) at asymptotic momentum $k_1 = 1.267$ a.u. and $k_2 = 2.749$ a.u., respectively. The effective momentum, which accounts for the Coulomb effect, can be calculated by $k_{\text{eff}} = [2(k^2/2 - E_g)]^{1/2}$. We obtain that $k_{1\text{eff}} = 1.844$ a.u. and $k_{2\text{eff}} = 3.058$ a.u., respectively. According to equation (3), these two adjacent minima correspond to

a phase variation of 2π . Thus, the retrieved internuclear distance is $R = 2\pi/(k_{2\text{eff}} - k_{1\text{eff}}) = 5.176$ a.u., which is pretty close to the actual value of 5.2 a.u.. Moreover, the solid line in figure 2(c) depicts the delay-dependent momentum $k(\tau)$ of one of the interference minima, which is determined by the phase difference between two nuclei upon ionization. One can see that $k(\tau)$ remains constant at the beginning and gradually decreases to $k = 2$ a.u. ($-4T_0$ to $4T_0$) when the laser-molecule interaction induces a phase difference between the two nuclei. When the IR pump is over, $k(\tau)$ maintains an oscillation similar to a sinusoidal function. Following the reconstruction procedure in section 2, the delay-dependent relative phase, given by $\Delta\phi(t_0) = [k_{\text{eff}}(t_0) - k_{\text{eff}}^s]R$, can be retrieved (dotted line) and compared with the TDSE simulated result (red solid line) as shown in figure 3(b). The time dependent electron occupation $|a(t_0)|^2$ in one of the nuclei can be also traced by calculating $[I(k)_{\text{max}} - I(k)_{\text{min}}]/[I(k)_{\text{max}} + I(k)_{\text{min}}]$ combined with the normalization condition $|a(t_0)|^2 + |b(t_0)|^2 = 1$. Figure 3(a) shows the reconstructed and simulated occupation. Both the reconstructed phase difference and occupation show excellent agreement with the simulated results, confirming the accuracy of our method.

The delay-dependent dynamics of the occupations and phase difference on the two nuclei can be interpreted by the laser-driven Rabi process as well. As shown in figure 3(a), the occupations are the same in the two nuclei around delay = $-8T_0$, which indicates that H_2^+ is in its ground state. Later, the formation of a superposition induced by the IR pump results in an oscillation. At delay = $-T_0$, the occupation oscillation has the largest contrast almost approaching unity, this indicates that $1s\sigma_g$ and $2p\sigma_u$ states have almost the same population and thus form a coherent superposition that leads to charge rapidly hopping between the two nuclei as shown in figure 3(a). Then the oscillation contrast gradually decreases and reaches a minimum at delay = $2T_0$, which corresponds to the maximum population of $2p\sigma_u$ state. Similar dynamics can be deduced from figure 3(b). The oscillating structure in figure 3(b) also indicates the formation of the $1s\sigma_g$ and $2p\sigma_u$ superposition. A π phase jump occurs at delay = $-T_0$, which means that the superposition is dominated by $2p\sigma_u$ state thereafter. Meanwhile, there is also a minimum of amplitude at

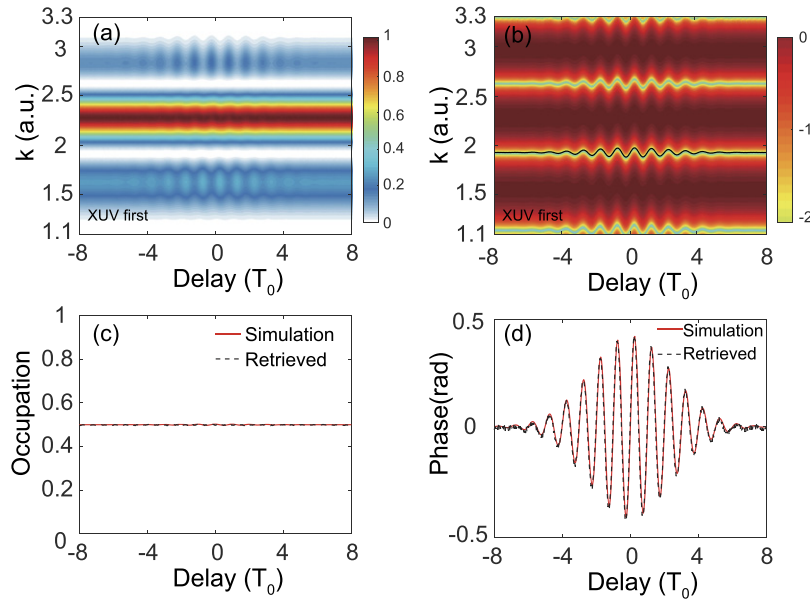


Figure 4. Reconstructed results of the charge migration in H_2^+ at $R = 10$ a.u. (a) and (b) are the same as figures 2(a)–(d) are the same as figures 3(a) and (b), except for a different internuclear distance.

delay = $2T_0$, when the phase difference is close to π as shown in figure 3(a). At this moment, electrons are almost evenly distributed in the two nuclei but with opposite signs in the wave function. This indicates that $2p\sigma_u$ is the dominant component at $2T_0$.

To demonstrate the universality of our approach, figure 4(a) shows photoelectron spectrum for a different internuclear distance $R = 10$ a.u.. The parameters of the pump and probe pulse remain the same. For the large internuclear distance case, strong coupling between the ground state and the first excited state emerges due to the charge-resonance effect [37]. Meanwhile, larger internuclear distance results in multiple interference minima in the spectrum. By substituting $R = 10$ a.u. into the cosine term in equation (3), we can obtain that two interference minima appear at $k = 1.5$ to $k = 3$ a.u., which leads to the three-peaked structure in the photoelectron spectra. Following the same procedure, $I(k)$ is obtained and displayed in figure 4(b). Four minima appear corresponding to different interference orders and the delay-dependent momentum of each minimum is almost the same. The delay dependent oscillation of each interference minimum represents the phase difference between the two nuclei, which is proportional to the vector potential of the IR pump [38]. The eigen-energy of the ground state is $E_g = -0.771$ a.u. at $R = 10$ a.u.. We extract the effective momenta for the two minima $k_1 = 1.914$ a.u. and $k_2 = 2.612$ a.u. and the reconstructed internuclear distance is $R = 10.28$ a.u.. The retrieved occupation and phase difference between two nuclei are displayed in figures 4(c) and (d), respectively, which are in excellent agreement with the TDSE simulation results. For both cases (figures 3 and 4) using different internuclear distances, R can be reconstructed with picometer spatial resolution. Meanwhile, the temporal resolution is only restricted to the delay step size of the pump–probe experiment, which is typically on the order of a few tens of attosecond [39, 40].

The method is presented within the fixed nuclear frame. In order to study how the delocalization of the nuclear wave packet would affect the reconstruction process, we statically add the contribution of the nuclear delocalization by calculating the interference patterns for a range of nuclear distances around $R_0 = 5.2$ a.u. and weighting them by a Gaussian probability distribution. The Gaussian distribution is given by $W(R, l) = e^{-2 \ln 2 * (R - R_0)^2 / l^2}$, where l represents the FWHM of the Gaussian distribution. The final photoelectron spectrum which considers this distribution is calculated by $I(k, \tau, l) = \sum |W(R, l)|^2 I(k, \tau, R)$. $I(k, \tau, R)$ represents the photoelectron spectrum of H_2^+ at fixed internuclear distance R . Figures 5(a) and (b) display the calculated spectrum for $l = 0.05$ a.u. and $l = 0.2$ a.u., respectively. The main spectral characteristics of these two spectra are the same as figure 2(a). However, it is obvious that the delocalization of the nuclear wave packet smears out the electronic dynamics and corresponding diffraction patterns, especially for figure 5(b). At delay = T_0 , destructive interference around $k = 2$ a.u. almost disappears. The charge migration of figures 5(a) and (b) is retrieved by our method and compared with the TDSE simulation results for fixed nuclear distance $R_0 = 5.2$ a.u. For $l = 0.05$ a.u., the retrieved occupation and phase difference (black dash line in figures 5(c) and (d)) are close to the fixed nuclear results. For $l = 0.2$ a.u., the delocalization effect results in a noticeable difference due to the smoothness of the interference minima. The evolution of the phase difference between the two nuclei (dotted line in figure 5(d)) however is less affected by the delocalization and can still be captured. Besides, nuclear motion induces and alters electronic coherences and populations via non-adiabatic couplings [41–43]. Although vibrational motion of nuclei reduces the electronic coherence, we consider it appropriate to ignore the vibrational motion for cases when the characteristic time scale of the charge migration process is much less than the vibration period [23].

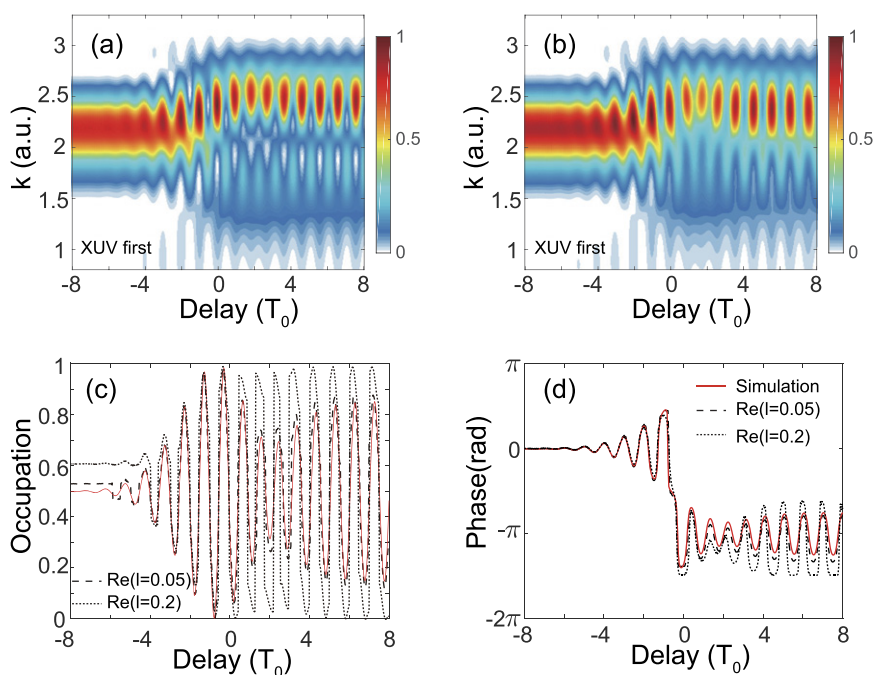


Figure 5. Analysis of the effect of the nuclear wave packet delocalization. (a) and (b) The calculated photoelectron spectrum for $l = 0.05$ a.u. and $l = 0.2$ a.u., respectively, where the delocalization is considered by using a Gaussian distribution. (c) and (d) The retrieved occupation and phase difference from (a) and (b) compare with the TDSE simulation results for fixed nuclear distance $R_0 = 5.2$ a.u. (red solid line). Black dash line for $l = 0.05$ a.u. and dotted line for $l = 0.2$ a.u..

Furthermore, a localized nuclear wavepacket such as the inner or outer turning points of a moving wavepacket is preferred for accurate dynamics reconstruction. More detailed and quantitative results require the establishment of a moving nuclei model, which will be subject to future study. We believe that the method has potential ability to monitor the molecular dissociation and electron localization [44]. For large molecules, the photoelectron distribution is determined by the symmetry of the initial state and the molecular geometry. In this case, multicenter interference will occur and the interference structures will become more complicated. Thus in order to probe the time-dependent charge location, further analysis on interference patterns in higher dimensional space will be required.

4. Conclusion

In conclusion, we have proposed a new method for imaging the laser-controlled charge migration in diatomic molecules by analyzing the interference patterns in the photoelectron spectrum. An IR pump pulse creates a time-dependent coherent superposition of electronic states and a subsequent linearly polarized XUV pulse is used to ionize the excited molecule. Based on a simple double-slit model, the interference patterns give access to the internuclear distance and also the time-dependent occupation of electron on each nucleus and phase difference of the electron wave function on the two nuclei. Such information completely determines the charge migration. The accuracy of this method is confirmed by comparing with TDSE simulated results at different internuclear distances, $R = 5.2$ a.u. and $R = 10$ a.u., respectively. This method

has potential ability to monitor the electron charge migration during nuclear motion and provides a new thought to trace the electron motion for large molecules.

Acknowledgments

This research was supported by the National Key Research and Development Program under Grant No. 2017YFE0116600, National Natural Science Foundation of China under Grant Nos. 11774111 and 12021004.

Data availability statement

All data that support the findings of this study are included within the article (and any supplementary files).

ORCID iDs

Xi Chen <https://orcid.org/0000-0003-3000-4929>
Wei Cao <https://orcid.org/0000-0003-3354-711X>

References

- [1] Goulielmakis E *et al* 2010 Real-time observation of valence electron motion *Nature* **466** 739–43
- [2] Holler M, Schapper F, Gallmann L and Keller U 2011 Attosecond electron wave-packet interference observed by transient absorption *Phys. Rev. Lett.* **106** 123601

- [3] Ott C *et al* 2014 Reconstruction and control of a time-dependent two-electron wave packet *Nature* **516** 374–8
- [4] Yakovlev V S, Gagnon J, Karpowicz N and Krausz F 2010 Attosecond streaking enables the measurement of quantum phase *Phys. Rev. Lett.* **105** 073001
- [5] Schultze M *et al* 2010 Delay in photoemission *Science* **328** 1658–62
- [6] Ossiander M *et al* 2017 Attosecond correlation dynamics *Nat. Phys.* **13** 280–5
- [7] Remetter T *et al* 2006 Attosecond electron wave packet interferometry *Nat. Phys.* **2** 323–6
- [8] Mauritsson J *et al* 2010 Attosecond electron spectroscopy using a novel interferometric pump–probe technique *Phys. Rev. Lett.* **105** 053001
- [9] Gruson V *et al* 2016 Attosecond dynamics through a Fano resonance: monitoring the birth of a photoelectron *Science* **354** 734–8
- [10] Cederbaum L S and Zobeley J 1999 Ultrafast charge migration by electron correlation *Chem. Phys. Lett.* **307** 205–10
- [11] Mignolet B, Levine R D and Remacle F 2014 Charge migration in the bifunctional PENNA cation induced and probed by ultrafast ionization: a dynamical study *J. Phys. B: At. Mol. Opt. Phys.* **47** 124011
- [12] Kraus P M *et al* 2015 Measurement and laser control of attosecond charge migration in ionized iodoacetylene *Science* **350** 790–5
- [13] Wörner H J *et al* 2017 Charge migration and charge transfer in molecular systems *Struct. Dyn.* **4** 061508
- [14] He M, Li Y, Zhou Y, Li M, Cao W and Lu P 2018 Direct visualization of valence electron motion using strong-field photoelectron holography *Phys. Rev. Lett.* **120** 133204
- [15] Belshaw L, Calegari F, Duffy M J, Trabattoni A, Poletto L, Nisoli M and Greenwood J B 2012 Observation of ultrafast charge migration in an amino acid *J. Phys. Chem. Lett.* **3** 3751–4
- [16] Blaga C I, Xu J, DiChiara A D, Sistrunk E, Zhang K, Agostini P, Miller T A, DiMauro L F and Lin C D 2012 Imaging ultrafast molecular dynamics with laser-induced electron diffraction *Nature* **483** 194–7
- [17] Wolter B *et al* 2016 Ultrafast electron diffraction imaging of bond breaking in di-ionized acetylene *Science* **354** 308–12
- [18] Xu J *et al* 2012 Laser-induced electron diffraction for probing rare gas atoms *Phys. Rev. Lett.* **109** 233002
- [19] Gaumnitz T, Jain A, Pertot Y, Huppert M, Jordan I, Ardana-Lamas F and Wörner H J 2017 Streaking of 43-attosecond soft-x-ray pulses generated by a passively CEP-stable mid-infrared driver *Opt. Express* **25** 27506–18
- [20] Zhao X, Wang S J, Yu W W, Wei H, Wei C, Wang B, Chen J and Lin C D 2020 Metrology of time-domain soft x-ray attosecond pulses and reevaluation of pulse durations of three recent experiments *Phys. Rev. Appl.* **13** 034043
- [21] Li J *et al* 2017 53-attosecond x-ray pulses reach the carbon K-edge *Nat. Commun.* **8** 186
- [22] Cousin S L, Di Palo N, Buades B, Teichmann S M, Reduzzi M, Devetta M, Kheifets A, Sansone G and Biegert J 2017 Attosecond streaking in the water window: a new regime of attosecond pulse characterization *Phys. Rev. X* **7** 041030
- [23] Yuan K-J and Bandrauk A D 2019 Ultrafast x-ray photoelectron imaging of attosecond electron dynamics in molecular coherent excitation *J. Phys. Chem. A* **123** 1328–36
- [24] Mukamel S, Piryatinski A and Chernyak V 1999 Two-dimensional Raman echoes: femtosecond view of molecular structure and vibrational coherence *Acc. Chem. Res.* **32** 145–54
- [25] Odenweller M *et al* 2011 Strong field electron emission from fixed in space H_2^+ ions *Phys. Rev. Lett.* **107** 143004
- [26] Yuan K J, Lu H and Bandrauk A D 2011 Linear- and circular-polarization photoionization angular distributions in $H_2H_2^+$ and by attosecond XUV laser pulses *Phys. Rev. A* **83** 043418
- [27] Yuan K J and Bandrauk A D 2012 Molecular above-threshold-ionization angular distributions with intense circularly polarized attosecond XUV laser pulses *Phys. Rev. A* **85** 053419
- [28] Niikura H, Légaré F, Hasbani R, Bandrauk A D, Ivanov M Y, Villeneuve D M and Corkum P B 2002 Sub-laser-cycle electron pulses for probing molecular dynamics *Nature* **417** 917–22
- [29] Landers A L, Wells E, Osipov T, Carnes K D, Alnaser A S, Tanis J A, McGuire J H, Ben-Itzhak I and Cocke C L 2004 Interference effects in double ionization of spatially aligned hydrogen molecules by fast highly charged ions *Phys. Rev. A* **70** 042702
- [30] Cohen H D and Fano U 1966 Interference in the photoionization of molecules *Phys. Rev.* **150** 30–3
- [31] Lennard-Jones J E 1929 The electronic structure of some diatomic molecules *Trans. Faraday Soc.* **25** 668–86
- [32] Lein M, Hay N, Velotta R, Marangos J P and Knight P L 2002 Interference effects in high-order harmonic generation with molecules *Phys. Rev. A* **66** 023805
- [33] Hermann M R and Fleck J A 1988 Split-operator spectral method for solving the time-dependent Schrödinger equation in spherical coordinates *Phys. Rev. A* **38** 6000–12
- [34] Chelkowski S and Bandrauk A D 1996 Wave-function splitting technique for calculating above-threshold ionization electron spectra *Int. J. Quantum Chem.* **60** 1685–9
- [35] Wang F, Liu K, Zhang X, Wang Z, Qin M, Liao Q and Lu P 2019 Attosecond streaking spectrum in the photoionization of the hydrogen molecular ion *Phys. Rev. A* **100** 043405
- [36] Itatani J, Quéré F, Yudin G L, Ivanov M Y, Krausz F and Corkum P B 2002 Attosecond streak camera *Phys. Rev. Lett.* **88** 173903
- [37] Mulliken R S 1939 Intensities of electronic transitions in molecular spectra II. Charge-transfer spectra *J. Chem. Phys.* **7** 20–34
- [38] Ivanov M Y and Corkum P B 1993 Generation of high-order harmonics from inertially confined molecular ions *Phys. Rev. A* **48** 580–90
- [39] Chini M, Mashiko H, Wang H, Chen S, Yun C, Scott S, Gilbertson S and Chang Z 2009 Delay control in attosecond pump–probe experiments *Opt. Express* **17** 21459–64
- [40] Yang Z, Cao W, Mo Y, Xu H, Mi K, Lan P, Zhang Q and Lu P 2020 All-optical attosecond time domain interferometry *Natl. Sci. Rev.* **nwaa211**
- [41] Kobayashi Y, Chang K F, Zeng T, Neumark D M and Leone S R 2019 Direct mapping of curve-crossing dynamics in IBr by attosecond transient absorption spectroscopy *Science* **365** 79–83
- [42] Kowalewski M, Bennett K, Dorfman K E and Mukamel S 2015 Catching conical intersections in the act: monitoring transient electronic coherences by attosecond stimulated x-ray Raman signals *Phys. Rev. Lett.* **115** 193003
- [43] Simmermacher M, Henriksen N E, Møller K B, Moreno Carrascosa A and Kirrander A 2019 Electronic coherence in ultrafast x-ray scattering from molecular wave packets *Phys. Rev. Lett.* **122** 073003
- [44] Kling M F *et al* 2006 Control of electron localization in molecular dissociation *Science* **312** 246–8